Available online at www.sciencedirect.com
SCIENCE DIRECT
Dyes and Pigments 73 (2007) 13–18
DYES and PIGMENTS
www.elsevier.com/locate/dyepig

Structure and colour properties in the Egyptian Blue Family, $M_{1-x}M'_xCuSi_4O_{10}$, as a function of M, M′ where M, M′ = Ca, Sr and Ba

E. Kendrick, C.J. Kirk, S.E. Dann*

Department of Chemistry, Loughborough University, Loughborough, Leicestershire LE11 3TU, United Kingdom

Received 6 July 2005; received in revised form 28 September 2005; accepted 7 October 2005
Available online 5 December 2005

Abstract

Solid solutions in the Egyptian Blue Family, $M_{1-x}M'_xCuSi_4O_{10}$, where M, M′ are the alkali-earth cations Ca, Sr and Ba, have been successfully synthesised from stoichiometric mixtures of silica, alkali-earth metal carbonates and copper carbonate at high temperature using solid state reactions. The structure of the blue products has been determined by Rietveld analysis using high quality powder X-ray diffraction data. As the average size of the cations on the alkali-earth metal site increases, the cell parameters also increase, although the variation occurs in an anisotropic manner due to the flexibility of the structure. UV–vis spectra and colour coordinate data were collected on the materials to correlate the changes in the structure with the observed colour properties. A concomitant reduction in lightness indicating potential weakening of the tinting capability is observed as the cell parameters lengthen. Prolonged exposure to natural light has a deleterious effect on the colour of these synthetic materials in a similar way to the natural minerals.

Keywords: Egyptian Blue; Rietveld refinement; Colour properties

1. Introduction

The layered copper silicates; cuprorivaite ($CaCuSi_4O_{10}$), wesselsite ($SrCuSi_4O_{10}$) and effenbergerite ($BaCuSi_4O_{10}$) are natural occurring silicate sheet minerals [1–3]. Cuprorivaite (Egyptian Blue) and effenbergerite (Hans Blue) have been used as blue pigments since ancient times and historic samples of these pigments have been investigated by a number of authors using both spectroscopy and X-ray diffraction [4–6]. The original composition of cuprorivaite was determined by Fouque [7] by the chemical analysis of single crystals of the material. Later, powder diffraction data were reported by Jope and Huse [8] for several powdered natural samples, although no intensity data were reported. More recently, these minerals have been synthesised and characterised by both X-ray and neutron diffraction [9,10], and their colour properties have been investigated [11]. Early studies by Pabst [9] gave poorly defined parameters for the silicate layers of cuprorivaite due to the complexity of the structure and the quantity of light atoms. Powder neutron diffraction data were used to successfully refine the structures and accurately determine the light atom positions using Rietveld methods by Hughes et al. [10] for $MCuSi_4O_{10}$ where M is a single alkali-earth cation. The layered copper silicates, [$MCuSi_4O_{10}$] where M is either Ca, Sr or Ba, are isostructural and crystallise in the tetragonal space group $P4/ncc$, $Z = 4$. The cell parameters increase anisotropically with the changing alkali-earth metal cation, where a decreases much less rapidly than c. The calcium analogue has cell parameters of $a = 7.30$ Å, $c = 15.10$ Å, while for strontium: $a = 7.37$ Å, $c = 15.59$ Å and for barium: $a = 7.44$ Å, $c = 16.14$ Å [10]. The structure

* Corresponding author.
E-mail address: s.e.dann@lboro.ac.uk (S.E. Dann).

0143-7208/$ - see front matter © 2005 Elsevier Ltd. All rights reserved.
doi:10.1016/j.dyepig.2005.10.006

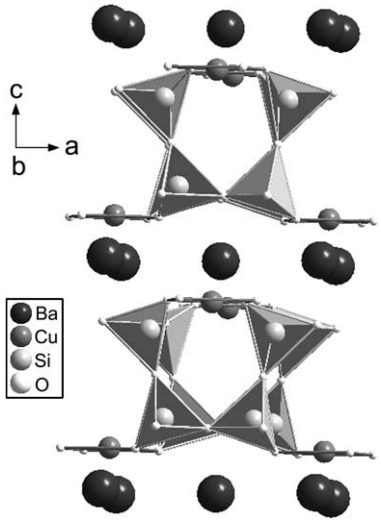

Fig. 1. Layered structure of $BaCuSi_4O_{10}$ showing silica ring network connected by square-planar coordinated copper, interspersed by barium cations.

is composed of rings of four SiO_4 tetrahedra, $[Si_4O_{10}]^{4-}$, which are linked together by square-planar coordinated copper. Each SiO_4 tetrahedron is connected to two neighbouring tetrahedra in the same ring and a third from a different ring. The rings are connected together by square-planar coordinated copper to form double copper silicate layers which are joined by alkali-earth cations in a distorted cubic geometry. The incorporation of different alkali-earth metal cations is possible due to the flexibility of the layered structure. (Fig. 1). One phenomenon that has been observed in the natural materials, is that bright natural light can cause dulling of the colour of these materials [12]. The chemical cause of this darkening has not been identified.

This work investigates the structural and colour properties of $(M_{1-x}M_x)CuSi_4O_{10}$ materials containing solid solutions of the alkali-earth cations, in order to obtain a greater understanding of the colour mechanism and the structural stability of these materials. The effect of strong light sources on the samples was also examined to generate a hypothesis to explain the colour loss in bright light.

2. Experimental

$(M_{1-x}M_x)CuSi_4O_{10}$ where M and M′ are Ca, Sr or Ba have been synthesised using conventional solid state reactions. SiO_2, $CaCO_3$, $SrCO_3$, $BaCO_3$ and $CuCO_3$ in the correct stoichiometric proportions were ground in a pestle and mortar to form a homogeneous mixture. The mixture was placed in alumina boats and fired at 1000 °C for 16 h. After cooling the products were reground and refired at 1000 °C for another 16 h. The products were washed initially by stirring in concentrated HCl to remove any unreacted starting materials, followed by washing with distilled water and then air dried.

Preliminary powder X-ray diffraction data were collected on a Phillips X'pert diffractometer operating with copper radiation using a 0.02° 2θ step in the 2θ range 20–60° over a period of 40 min with a scintillation counter to determine sample purity. Although it was possible to form a solid solution across the whole series of x for a mixture of both calcium and strontium or strontium and barium cations, it was not possible to produce a solid solution consisting of a mixture of calcium and barium cations. In the latter case, a dual phase system containing the barium and calcium end members was always produced. High quality powder X-ray diffraction data were collected in the 2θ range 10–100° with a step size of 0.015° over a period of 13 h for the Ca/Sr and Sr/Ba series for Rietveld analysis. Scanning electron microscopy was performed on both series to investigate the size and shape of the particles and EDX was used to confirm the ratio of the alkali-earth cations. Diffuse reflectance UV–vis were collected on undiluted ground powdered samples over a range 300–1000 nm using Perkin Elmer Lambda 35 Spectrophotometer operating with WINLAB 4.2 software and colour parameters were determined using Colour Methods V3 software. The data were corrected using the Kubelka–Munk function in order to obtain absorption maxima, and normalised to the highest intensity. IR data were collected on pressed KBr disks over the range 4000–500 cm^{-1} using a Perkin Elmer FT 180. Raman data were collected on a Jobin-Yvon LabRam 80 HR fitted with confocal microscope and xy mapping stage using the 20 mW 633 nm laser line of a HeNe laser.

Table 1
Refined unit cell and fit parameters, derived bond lengths and UV maxima for the $Ca_{1-x}Sr_xCuSi_4O_{10}$ series

x	R_{wp}	χ^2	a (Å)	c (Å)	M–O1 (Å)	M–O2 (Å)	Cu–O (Å)	Absorption maxima (nm)	
0	0.039	4.28	7.3032(6)	15.133(1)	2.385(3)	2.713(3)	1.922(3)	626	794
0.01	0.05	6.68	7.2995(7)	15.129(1)	2.374(4)	2.708(4)	1.909(4)	627	793
0.015	0.0492	5.24	7.3008(6)	15.133(1)	2.378(4)	2.718(4)	1.908(4)	627	792
0.02	0.0504	7.03	7.3045(9)	15.143(2)	2.365(4)	2.745(4)	1.921(4)	627	792
0.1	0.0533	7.81	7.308(1)	15.180(3)	2.393(5)	2.692(5)	1.916(5)	627	794
0.2	0.0448	4.29	7.3074(8)	15.212(2)	2.396(4)	2.715(4)	1.915(4)	630	799
0.3	0.0365	3.65	7.3092(7)	15.264(1)	2.425(4)	2.714(3)	1.923(3)	629	798
0.4	0.0483	6.81	7.323(2)	15.337(3)	2.392(7)	2.663(6)	1.950(6)	629	797
0.5	0.0365	3.77	7.3270(7)	15.355(1)	2.463(4)	2.738(3)	1.917(3)	628	803
0.6	0.0389	4.30	7.3309(9)	15.395(2)	2.466(4)	2.749(3)	1.920(4)	626	801
0.7	0.0388	4.56	7.3435(8)	15.456(2)	2.495(4)	2.752(3)	1.891(4)	627	799
0.8	0.0342	3.53	7.3493(6)	15.496(1)	2.495(3)	2.756(3)	1.921(3)	626	801
0.9	0.0336	3.39	7.3569(4)	15.541(1)	2.527(3)	2.775(2)	1.930(3)	626	799
1	0.0448	6.03	7.3723(5)	15.593(1)	2.560(4)	2.795(3)	1.920(3)	624	799

Table 2
Refined atomic and fit parameters, derived bond lengths and UV maxima for the $Sr_{1-x}Ba_xCuSi_4O_{10}$ series

x	R_{wp}	χ^2	a (Å)	c (Å)	M–O1 (Å)	M–O2 (Å)	Cu–O (Å)	Absorption maxima (nm)	
0	0.0448	6.03	7.3723(5)	15.593(1)	2.560(4)	2.795(3)	1.920(3)	623	801
0.1	0.0526	7.21	7.3695(6)	15.640(1)	2.564(5)	2.804(4)	1.906(5)	626	803
0.2	0.0453	4.88	7.3816(7)	15.713(1)	2.604(5)	2.835(4)	1.923(4)	626	805
0.3	0.0556	6.76	7.384(1)	15.775(2)	2.627(7)	2.865(5)	1.907(5)	628	811
0.4	0.0487	3.50	7.3932(9)	15.842(2)	2.652(7)	2.867(5)	1.912(5)	628	811
0.5	0.0584	5.97	7.3925(7)	15.886(2)	2.679(7)	2.888(5)	1.921(5)	631	817
0.6	0.0413	2.75	7.4011(5)	15.942(1)	2.687(5)	2.894(4)	1.919(4)	630	817
0.7	0.0413	2.75	7.4116(6)	16.005(1)	2.714(6)	2.897(4)	1.930(5)	630	817
0.8	0.0394	2.39	7.4187(4)	16.044(1)	2.738(4)	2.906(3)	1.915(3)	629	821
0.9	0.0579	4.62	7.4287(5)	16.087(1)	2.762(7)	2.895(4)	1.936(5)	628	818
1	0.0546	4.18	7.4378(3)	16.124(6)	2.795(5)	2.929(4)	1.920(4)	627	820

3. Results and discussion

3.1. X-ray refinement

Rietveld refinements were performed on the data using the GSAS [13] suite of programs. Initial stages of refinement included background and profile parameters. Starting atomic parameters were taken from Pabst [9] and occupancies for the alkali-metal cations were set at the theoretical values as confirmed by EDX. The atomic parameters were added sequentially to the refinement starting with the heavy atoms. Isotropic temperature factors were then included for all atoms. All the refinements converged smoothly. Final atomic parameters are given in Table 1, and important bond lengths in Table 2. A typical refinement profile is given in Fig. 2.

3.2. Calcium–strontium series

The cell parameters increase anisotropically as the amount of strontium in the solid solution increases. The cell parameter a increases as a power function while the cell dimension c increases linearly. The increase in cell size with amount of strontium in the solid solution is shown in Fig. 3 and the increase in volume with respect to x is shown in Fig. 4. It is clear from the data tables that while the Cu–O bond lengths remain constant at approximately 1.9 Å, the alkaline-earth metal cation bond lengths increase with increasing strontium levels. This shows that replacing calcium with strontium has little effect on the bond distances within the $[Si_4O_{10}]^{4-}$ring, where the copper square-plane links four of these units together.

Since the Si–O bond lengths also remain constant at 1.6 Å, it is apparent that the double layers are relatively unaffected by the changing alkali-earth metal cation. In contrast, the two bond lengths around the eight-fold alkali-earth metal cation clearly lengthen as the larger strontium cation replaces the smaller calcium cation (Fig. 5). This lengthening occurs in an anisotropic manner, where the bonding interaction to the oxygen involved in the copper–oxygen square-plane lengthens more rapidly than the alkali-metal–O bonding interaction to the oxygen within the Si–O ring. A typical UV–vis

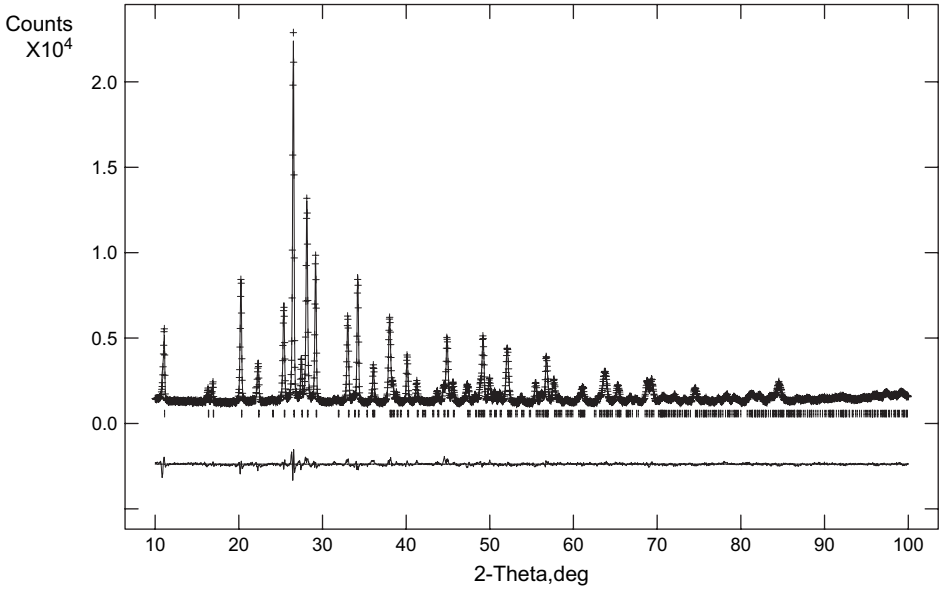

Fig. 2. Rietveld refinement profile of $Sr_{1-x}Ba_xCuSi_4O_{10}$ $x = 0.5$. The upper crossed line represents the experimental data, the upper solid line the calculated pattern and the lower solid line represents the difference between the calculated and experimental data.

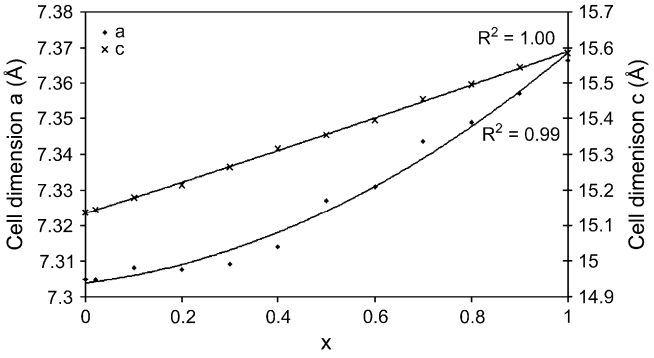

Fig. 3. Anisotropic change in lattice parameters a and c of $Ca_{1-x}Sr_xCuSi_4O_{10}$ with x.

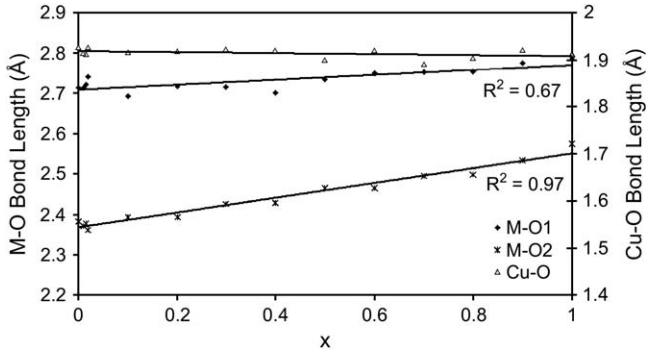

Fig. 5. Change in derived metal–oxygen bond lengths in $Ca_{1-x}Sr_xCuSi_4O_{10}$ with x.

electronic spectrum for the Ca/Sr series for the $Ca_{0.5}Sr_{0.5}CuSi_4O_{10}$ sample is shown in Fig. 6 and is similar to those obtained previously [10,14,15]. The three broad transitions observed in the visible region originate from d–d transitions which are weakly allowed, despite approximate D_{4h} symmetry at the copper centre, due to vibronic coupling. The three transitions occur in near identical wavelengths in the series at 800 nm ($^2B_{1g} \rightarrow {}^2B_{2g}$), 630 nm ($^2B_{1g} \rightarrow {}^2E_g$) and 540 nm ($^2B_{1g} \rightarrow {}^2A_{1g}$).

IR data collected in the region 500–4000 cm^{-1} show a strong absorption in the silicate region at 700–800 cm^{-1}. A graphical representation of these data is given in Fig. 7 along with the data from the UV–vis experiment for the major absorption. The IR band shows a slight shift to higher wavenumber as more strontium is added to the system. Due to the breadth of the absorptions, it is difficult to ascertain whether a similar trend is observed in the UV–vis spectra, particularly for the two overlapping bands. However, the band at longest wavelength does appear to show a slight shift to longer wavelength as the strontium doping increases. Colour parameters for these systems are summarised in Table 3 and indicate no obvious trend in the colour parameters although a visible lightening of the colour of the sample is apparent with the naked eye. Attempts were also made to record the Raman data using the 633 nm laser line but only poor quality data could be collected. Examination of the samples after treatment with the laser showed that the samples were dotted with grey spots. The reason for this colour loss is discussed in further detail later, vide infra.

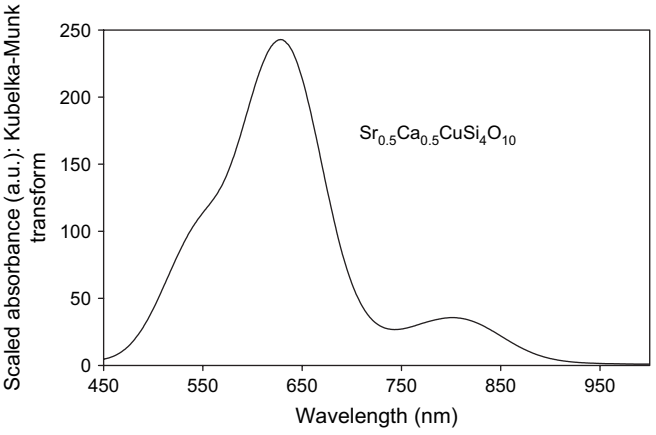

Fig. 6. Kubelka–Munk corrected UV–vis spectrum of the $Ca_{0.5}Sr_{0.5}CuSi_4O_{10}$ series.

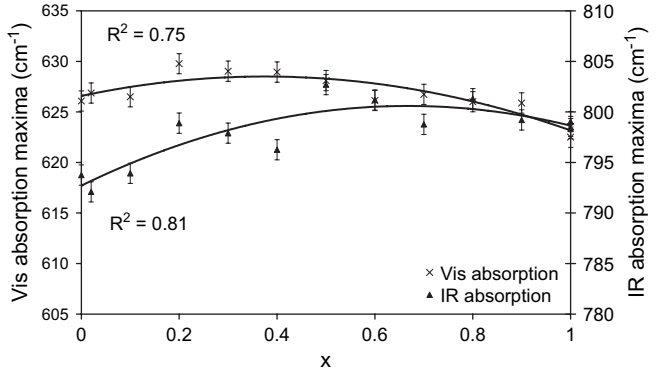

Fig. 7. Change in position of absorption maxima for UV–vis and IR spectra of $Ca_{1-x}Sr_xCuSi_4O_{10}$ with x.

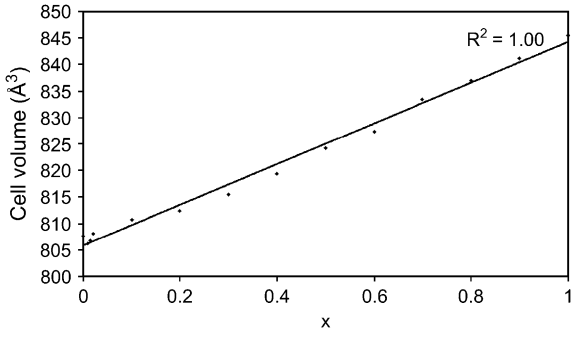

Fig. 4. Isotropic change in cell volume of $Ca_{1-x}Sr_xCuSi_4O_{10}$ with x.

3.3. Strontium–barium series

The structural behaviour observed in the calcium–strontium series is mirrored in the strontium–barium series, where the cell parameters behave anisotropically across the series. The cell parameters, a and c, increase anisotropically as the level of barium in the solid solution increases from $a = 7.36$, $c = 15.59$ where $x = 0$ to $a = 7.44$, $c = 16.12$ for $x = 1$. However, as in the calcium–strontium series, the cell volume increases linearly with increasing barium content as shown

Table 3
L^*, a^*, b^* colour parameters for the $M_{1-x}M'_xCuSi_4O_{10}$ series

Formula	L^*	a^*	b^*
$SrCuSi_4O_{10}$	82.79	−6.50	−23.52
$Sr_{0.8}Ba_{0.2}CuSi_4O_{10}$	81.80	−7.02	−24.55
$Sr_{0.6}Ba_{0.4}CuSi_4O_{10}$	78.57	−7.11	−28.59
$Sr_{0.4}Ba_{0.6}CuSi_4O_{10}$	77.31	−7.53	−28.19
$Sr_{0.2}Ba_{0.8}CuSi_4O_{10}$	75.07	−7.53	−29.76
$BaCuSi_4O_{10}$	76.23	−7.98	−29.91
$CaCuSi_4O_{10}$	86.54	−4.62	−17.40
$Ca_{0.8}Sr_{0.2}CuSi_4O_{10}$	81.68	−4.10	−18.49
$Ca_{0.6}Sr_{0.4}CuSi_4O_{10}$	84.44	−4.46	−19.24
$Ca_{0.4}Sr_{0.6}CuSi_4O_{10}$	83.19	−4.59	−19.49
$Ca_{0.2}Sr_{0.8}CuSi_4O_{10}$	85.94	−4.90	−18.65
$SrCuSi_4O_{10}$	82.79	−6.50	−23.52

in Figs. 8 and 9. Similarly, the geometry of the species within the silicate double layer remains relatively unchanged, while the distance between the layers increases to accommodate the larger alkali-earth metal cation. Although both strontium–barium and calcium–strontium give a solid solution across the full series of x, no sign of a solid solution was ever observed between calcium and barium for any value of x. The likely cause of this must be due to the difference in size of the cations. Since these cations are acting as a spacer between the layers and no major structural change occurs within the silicate layers, it can be hypothesised that the large size mismatch between calcium and barium could cause an instability in the structure causing phase separation, where the difference between the Ca–O and Ba–O bond lengths is substantial (∼0.4 Å).

Alkali-metal–oxygen bond lengths change in a similar fashion for the strontium–barium series as was observed in the calcium–strontium series, where a much larger change in the alkali-earth–O1 bond length is observed compared with the alkali-earth–O2 bond length (Fig. 10). A typical UV–vis reflectance spectrum for the barium–strontium series for the $Sr_{0.5}Ba_{0.5}CuSi_4O_{10}$ sample is shown in Fig. 11. The first maximum is shifted to higher wavenumber in comparison to the calcium–strontium series (Fig. 6). The three transitions occur in near identical wavelengths throughout the series at 820 nm ($^2B_{1g} \rightarrow {}^2B_{2g}$), 630 nm ($^2B_{1g} \rightarrow {}^2E_g$) and 540 nm ($^2B_{1g} \rightarrow {}^2A_{1g}$). There is possibly a small shift to higher

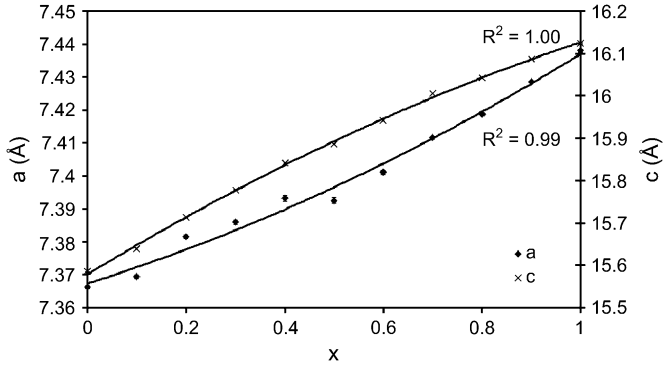

Fig. 8. Anisotropic change in lattice parameters a and c of $Sr_{1-x}Ba_xCuSi_4O_{10}$ with x.

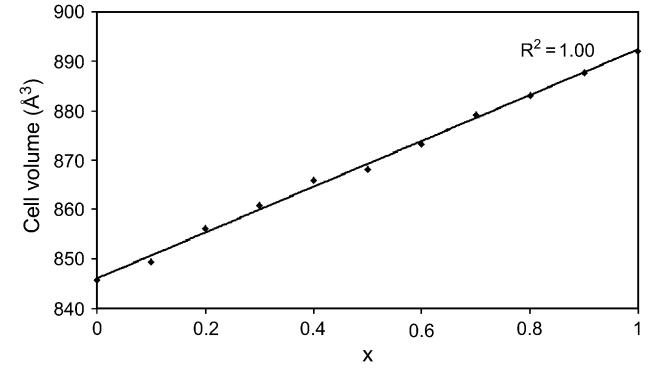

Fig. 9. Isotropic change in cell volume of $Sr_{1-x}Ba_xCuSi_4O_{10}$ with x.

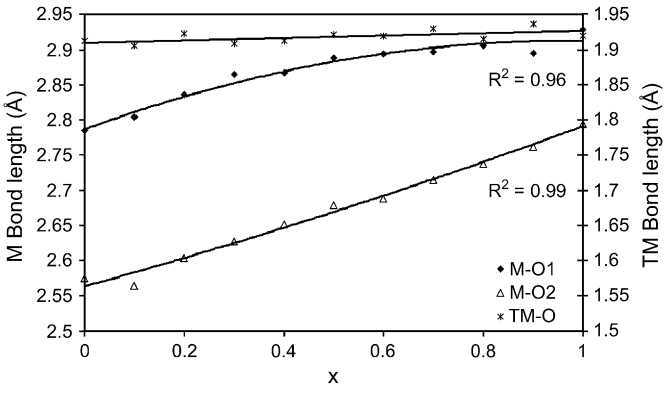

Fig. 10. Change in derived metal–oxygen bond lengths in $Sr_{1-x}Ba_xCuSi_4O_{10}$ with x.

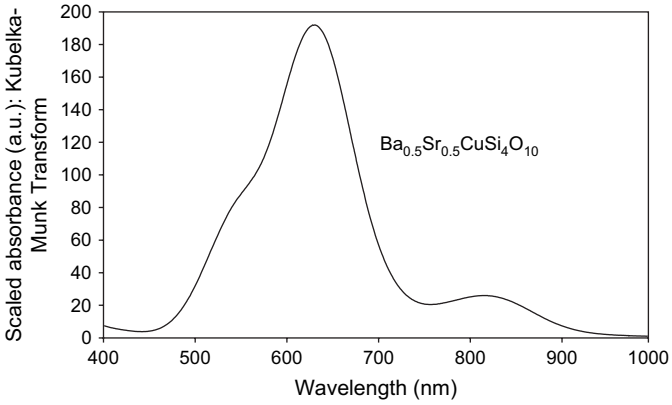

Fig. 11. Kubelka–Munk corrected UV–vis spectrum of the $Sr_{0.5}Ba_{0.5}CuSi_4O_{10}$ series.

wavenumber for the ($^2B_{1g} \rightarrow {}^2B_{2g}$) transition as indicated in Fig. 12, although due to the width and overlap of the bands, it is impossible to ascertain how accurately these bands can be deconvoluted. Unlike the data for the calcium–strontium series, the colour parameters of the strontium–barium series (Table 3) clearly show a correlation between the colour parameters and the cations within the unit cell. As the barium content increases there is an increase in the overall absorption of the sample and a decrease in the L^* value. There is also

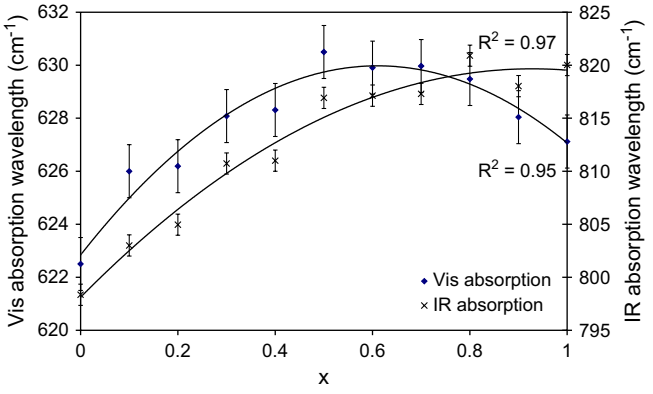

Fig. 12. Change in position of absorption maxima for UV–vis and IR spectra of $Sr_{1-x}Ba_xCuSi_4O_{10}$ with x.

a decrease in both the a^* colour coordinate, as it moves away from the red towards the blue, and the b^* coordinate as it moves through yellow towards the green. The samples visibly lighten in colour as the barium content increases. Samples left in bright sunlight for long periods (ca 12 weeks) showed a notable darkening with time, in comparison to those kept in a brown glass jar. Powder X-ray diffraction analysis of the light aged samples showed a small amount of copper oxide in the X-ray pattern after light exposure. Tenorite (CuO) has also been detected in powdered samples of natural Egyptian Blue [16] and was assumed to have been generated by aerial oxidation. However, since Egyptian Blue contains copper in the divalent state, it is more likely that the compound is showing light instability rather than air instability as confirmed by the colour loss caused by irradiation of the samples with high intensity laser light during the attempted Raman experiment. Degradation by bright light may therefore be the cause of the darkening observed in the historic samples [12].

References

[1] Jaksch H, Seipel W, Weiner KL, Elgoresy A. Naturwissen 1983;70:525.
[2] Giester G, Rieck B. Miner Mag 1994;58:663.
[3] Giester G, Rieck B. Miner Mag 1996;60:795.
[4] Mirti P, Appolonia A, Casoli A, Ferrari RP, Laurenti E, Canesi AA, et al. Spectrochim Acta A 1995;51:437.
[5] Edreira MC, Feliu MJ, Fernandex-Lorenzo C, Martin J. Helv Chim Acta 2003;86:29.
[6] Bouherour S, Berke H, Wiedemann HG. Chimia 2001;55:942.
[7] Fouque F. Bull Soc Fr Miner 1889;12:36.
[8] Jope EM, Huse G. Nature 1946;146:26.
[9] Pabst A. Acta Crystallogr 1959;12:733.
[10] Hughes EM, Pack MJ, Dann SE, Weller MT. An Quim 1997;93:233.
[11] Botto IL, Baran EJ, Minelli G. An Assoc Quim Argent 1987;75:429.
[12] Daniels V. Natural History Museum, Personal Communication.
[13] Larson AC, von Dreele R. GSAS 'Generalised structure analysis system'; 1986, MS805 LANSCE.
[14] Clark MG, Burns RG. J Chem Soc A 1967:1034.
[15] Clark MG, Burns RG. Inorg Chem 1966;5:1268.
[16] Pages-Camagna S, Colinart S, Coupry C. J Raman Spectrosc 1999; 30:313.